2023

Effect of Autoclave Process Parameters on Mechanical Behaviors of Carbon Fiber Reinforced Polymer Composites Fabricated via Additive Manufacturing

Quang Hao Nguyen
University of Central Florida

EFFECT OF AUTOCLAVE PROCESS PARAMETERS ON MECHANICAL BEHAVIORS OF CARBON FIBER REINFORCED POLYMER COMPOSITES FABRICATED VIA ADDITIVE MANUFACTURING

by

QUANG HAO NGUYEN

A thesis submitted in partial fulfillment of the requirements
for the program of Honors Undergraduate Thesis
in the Department of Mechanical and Aerospace Engineering
in the College of Engineering and Computer Science
at the University of Central Florida
Orlando, Florida

Spring Term
2023

Major Professor: Dazhong Wu

Abstract

Additively manufactured carbon fiber reinforced polymers (CFRP) are vastly studied for their remarkable mechanical properties compared to most other 3D printed materials. Different methods were employed to further increase mechanical performance of CFRP 3D printed parts. The objective of the study is to investigate the effect of autoclave postprocessing on the interlaminar shear behavior between 3D printed CFRP layers. 3D printed CFRP samples were processed with nine combinations of temperature and vacuum in an autoclave. Short beam shear (SBS) tests were performed to characterize the interlaminar shear strength (ILSS) of the samples after autoclave processing. Digital image correlation (DIC) was utilized to quantify the strain and failure mode of the samples during SBS tests. From SBS mechanical tests, the curing temperature and vacuum of 170 C and -90 kPa produced samples with the highest ILSS, 39 MPa, a 46% improvement compared to uncured samples. The observed failure modes were fracture and delamination. Little work in additive manufacturing has applied autoclave as a post-process procedure. This study aims to explore this technique and establish its viability in improving mechanical performance of 3D printed fiber-reinforced parts.

Acknowledgement

Firstly, I would like to thank Dr. Dazhong Wu for facilitating this project in his lab. Dr. Wu provided me with the opportunity and inspiration to develop and conduct this project. This endeavor would not have been possible without his guidance and encouragement.

I would like to extend my sincere thanks to Dr. Jihua Gou for providing the equipment that was crucial to this study. Many thanks to his lab manager, Christopher Valera, who sacrificed his time to help me meet intensive deadlines.

Finally, I would like to thank my parents for providing financial and material support throughout my undergraduate degree. Their support and trust gave me confidence to overcome any challenge on my way to achieving academic success.

TABLE OF CONTENTS

LIST OF FIGURES

LIST OF TABLES

1. Introduction

Additively manufactured (AM) carbon fiber reinforced polymer (CFRP) composites have been a topic of intensive study. This is due to their high strength-to-weight ratio provided by the carbon fiber and the cost effective, fast production time, and low material wastage advantage of AM. Comprehensive studies have been conducted to evaluate the effectiveness of different printing parameters such as fiber volume, printing orientation, layer height, and infill pattern to achieve the maximum mechanical properties on mechanical behaviors such as tensile, compressive, flexural and interlaminar shear strength (ILSS) of additively manufactured CFRP composites [1-3]. One common problem that the mentioned studies identified was the presence of voids within the matrix material and between the fibers. The effect of voids on the tensile properties of CFRP was studied [4]. Several researchers attempted to reduce the porosity of AM CFRP specimens with a compression mold [4], a compaction device [5] and a vacuum chamber [6]. The correlation between the reduced porosity and enhanced inter-layer bonding between the fibers and the matrix material was observed.

Conventionally manufactured carbon fiber parts must be post-processed in autoclaves to fully cure. This curing process is known to suppress void growth in the epoxy during the layup process [7]. Autoclave processing was used to post-process additively manufactured Kevlar reinforced nylon specimens [8]. The tensile strength of the post-processed specimens was double that of the unprocessed ones. However, the authors of the study only used one set of temperature and pressure in the autoclave process. The conclusion that autoclave processing enhanced the tensile strength due to the stronger fiber-matrix bonding was not quantified.

The aim of this study is to investigate the effect of autoclave process parameters on the interlaminar shear behavior of CFRP specimens, with a specific focus on determining how temperature and vacuum affect the ILSS of additively manufactured CFRP composites. Based on our literature review, our hypothesis is that an increase in autoclave temperature will lead to an increase in the ILSS. This is because high processing temperatures can reduce the internal voids of CFRP composites to improve adhesion between fibers and matrix materials. Similarly, as the vacuum level increases, the ILSS increases due to the vacuum bag compressing the embedded continuous carbon fiber, removing internal voids. However, when temperature and vacuum increase to a certain point, the compression from the vacuum bag will induce fiber pullout and breakage, leading to the deformation of the internal structure of CFRP samples, and thus decreasing the ILSS. Therefore, the goal of this study is to determine the optimal combination of temperature and vacuum to reduce the porosity and improve the mechanical properties of AM CFRP composites.

2. Literature Review

CFRP composites are carbon fibers coated with the matrix material of thermoplastic. The matrix materials are usually Polylactic Acid (PLA), Acrylonitrile Butadiene Styrene (ABS) or Nylon 6. The thermoplastic coating provides CFRP composites with melt processibility, which allows CFRP composites to be manufactured using AM. CFRP composites are divided into two groups: short and continuous CFRP composites. Short CFRP materials are thermoplastic filaments with chopped carbon fibers embedded along their length. Short CFRP composites have been applied in several 3D printing techniques including stereolithography (SLA), fused filament fabrication (FFF), selected laser sintering (SLS), and laminated object manufacturing (LOM). Continuous CFRP composites are continuous carbon fibers bundled together with a light coating of thermoplastic. Continuous CFRP composites are usually printed alongside short CFRP composites or thermoplastic materials to enhance the mechanical behavior of the 3D printed product. Continuous CFRP, however, is currently limited to material extrusion techniques.

For this study, continuous and short CFRP composites will be used to print testing specimens via fused deposition modelling (FDM) techniques. This technique involves extruding the filament onto the build bed of the 3D printer. The nozzle is heated up to just over the melting point of the material. This allows the material to flow through the nozzle and solidify immediately after the extrusion. The nozzle will extrude material in the x and y direction to print each layer. After one layer is done, the build bed lowers, and a new layer is deposited on top of the old one. This process continues until the product is complete. *Figure 1* demonstrates an FDM-based 3D printer that consists of two extruders. The 3D printer used in this study utilizes the same extruding

mechanism, where one extruder deposits the short CFRP matrix material, and the other extruder deposits the continuous CFRP for structural reinforcement.

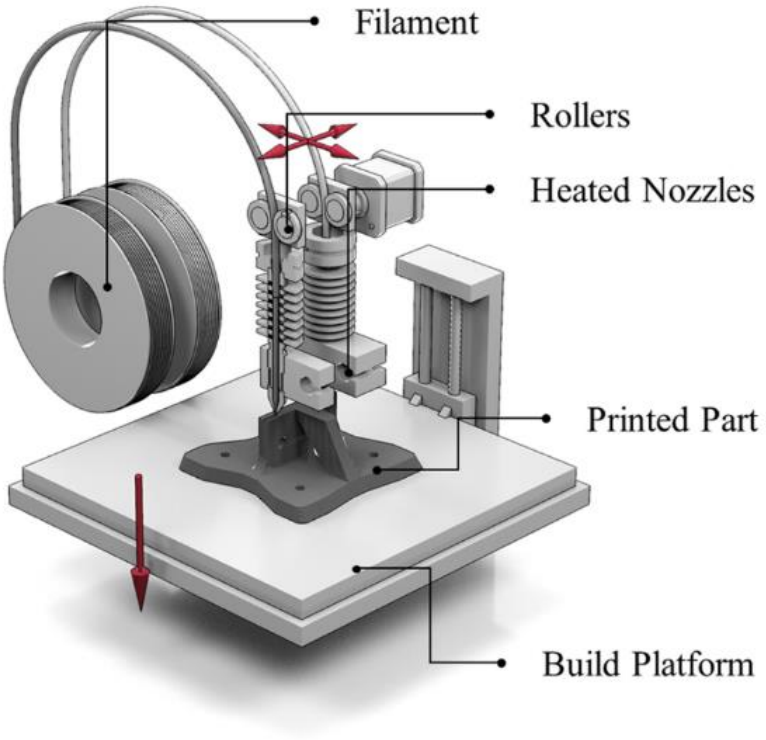

Figure 1: Schematic of fused filament fabrication using two materials. Red arrows indicate relative mechanical motion of components [9]

Studies about CFRP composites have been revolving around enhancing the mechanical properties of products through modifying printing parameters. One study investigated the effect of fiber type, fiber volume, and fiber orientation on the tensile and flexural behavior of CFRP composites [10]. Another study examined the effect of layer height and fiber volume on the interlaminar shear behavior of Nylon reinforced with carbon fiber, fiberglass, and Kevlar [3]. Some researchers developed a customized print path to simulate the woven pattern of conventionally manufactured carbon fiber and examined the product's tensile strength [11]. Tensile strength was also investigated under the influence of different infill densities, print speeds,

and layer heights [12]. One common problem that was identified in all the mentioned studies was the presence of voids within the filaments and pores between the deposited material. Since the extruded material has a circular cross section, the stacking of layers will introduce gaps at the layers' interface.

The mentioned defects in the 3D printed object originate from the filament manufacturing process and from the extrusion process, which is intrinsic to AM. Hence, little improvement in the printing process can be made to minimize the void size. Post-processing, however, has proven to help reduce the void content of testing coupons. Mechanical compaction stage, annealing, chemical treatment, and pressure treatment have been implemented and all yielded enhanced mechanical properties [13-16]. However, those studies either lacked the characterization of void content, did not investigate the interlayer bonding between fiber and matrix layers, or did not investigate combinations of multiple post-processing parameters. This study aims to reduce the void content of CFRP composites with a combination of temperature and pressure treatment which can be achieved with an autoclave.

3. Experimental Procedures

Additive manufacture process and materials

All the test specimens will be fabricated using the Markforged Mark Two printer. The printer has two extruders. One extruder prints short CFRP filament; the other extruder prints continuous CFRP. The short CFRP filament is the Markforged Onyx. Onyx is short carbon fiber/Nylon 6 matrix material filament proprietarily produced by Markforged. The nominal diameter of the Onyx filament is 1.75 mm. The continuous carbon fiber filament is provided by Markforged with the nominal diameter of 0.4 mm. *Figure 2* illustrates the schematic of dual extrusion system of the Mark Two 3D printer. The figure also shows the global printing coordinate (x, y, z) and the local material coordinate (0°, 90°) systems.

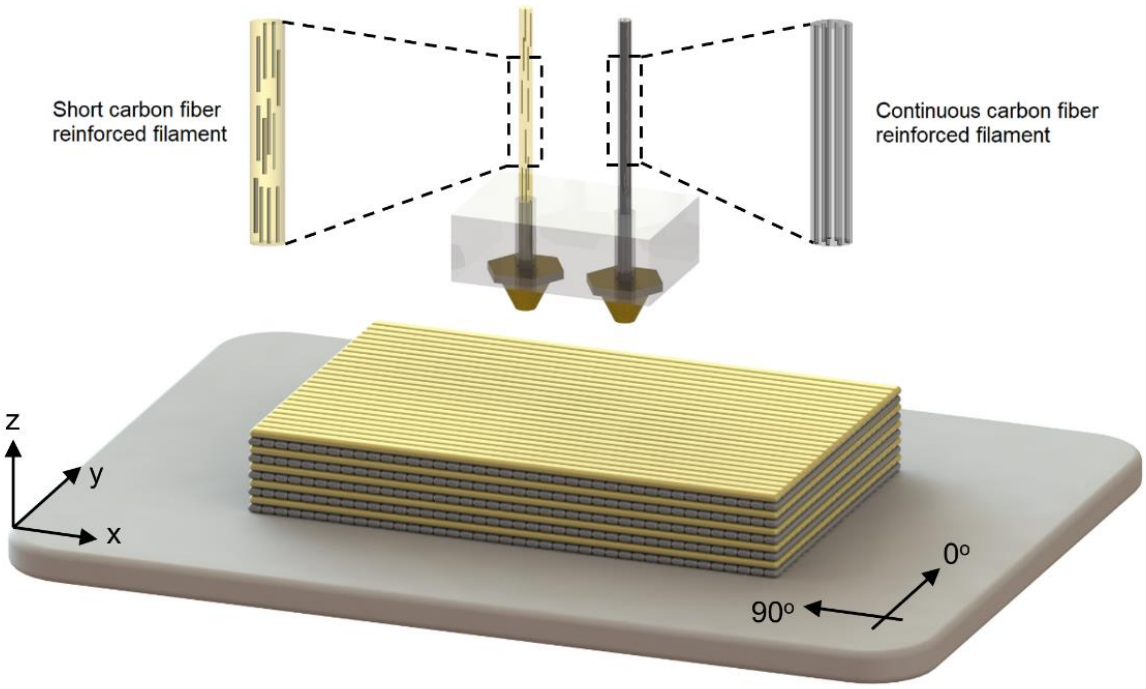

Figure 2: Schematic of dual extrusion system for short and continuous carbon fiber filaments

The short beam shear (SBS) samples were modeled in SolidWorks. The model was uploaded to the company's slicing software Eiger. The infill density is 100% with isotropic pattern with zero concentric fiber rings. The layer height for both short and continuous CFRP is 0.125 mm. The raster angle is 0° for the continuous CFRP filaments. This setting is to ensure the direction of the fiber is along the length of the specimen. The raster angle of the Onyx layers is set to 0° and 90°. The wall thickness is 0.4 mm. The first and last four layers are preset to be Onyx by the Eiger software. Between the fifth layer from the bottom and the fifth layer from the top inclusively, two layers of continuous CFRP are deposited, followed by two layers of Onyx. As a result, a total of twenty-two layers of continuous CFRP are embedded in each specimen. The nozzle temperatures for short and continuous CFRP are 275°C and 232°C, respectively. The printer's build bed is unheated and kept at room temperature of 75°F. *Figure 3* illustrates the described internal layup pattern for short and continuous CFRP filaments of SBS samples.

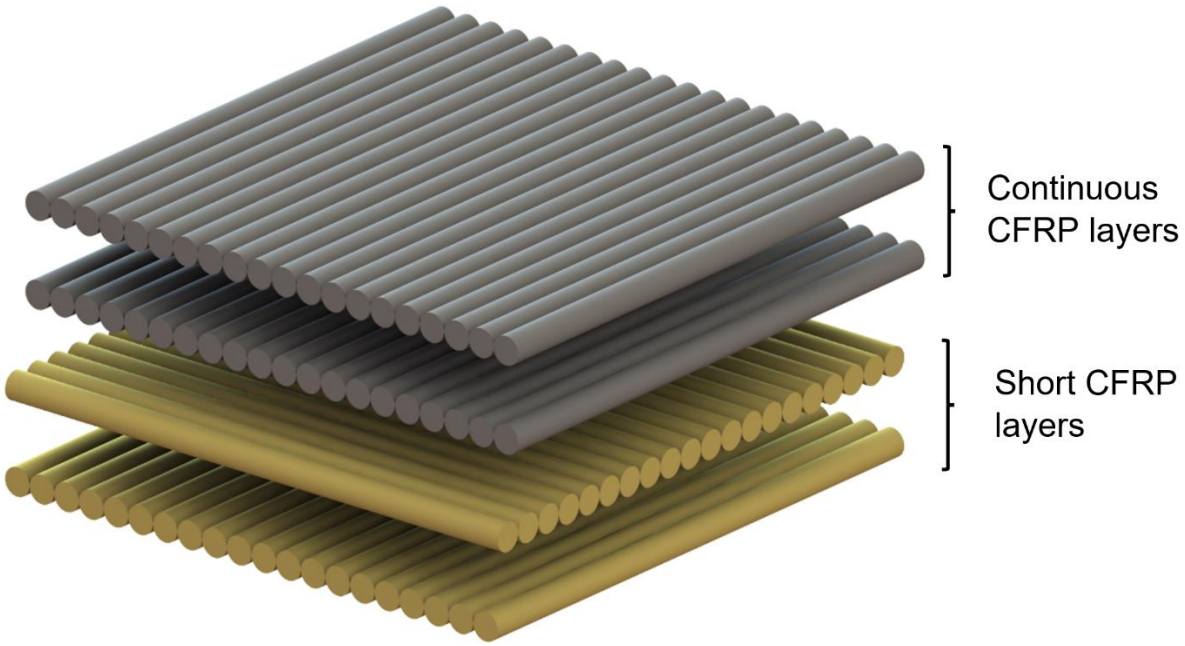

Figure 3: Internal layup pattern of short and continuous CFRP layers of SBS samples

Short beam shear specimens' fabrication

The testing standard of ASTM D2344 was followed to determine the interlaminar shear strength of 3D printed CFRP samples. The samples are in the form of a short beam. Samples are loaded in three-point bending. The standard provides different configurations of the testing beam. In this study, the samples will follow the flat specimen configuration in SI units. *Figure 4* below illustrates the dimensions and their ranges for the test beam. All dimensions are in millimeters. The figure also illustrates the raster printing pattern angle.

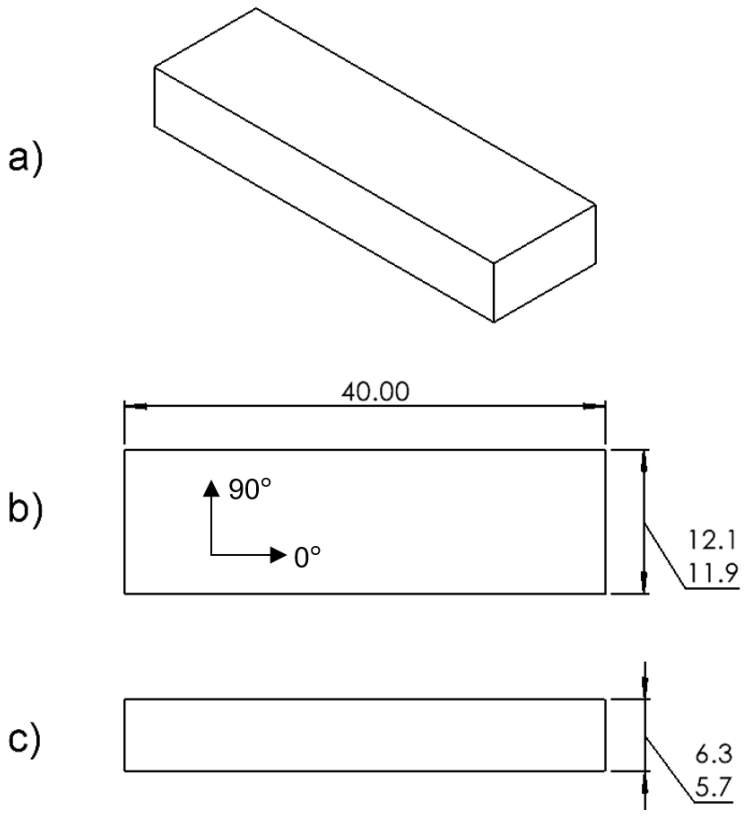

Figure 4: Dimensions of SBS samples according to ASTM D2344 standard; a) Isometric view, b) top view, and c) side view

All specimens were printed according to ASTM D2344 standard for short-beam shear (SBS) strength tests. Test samples are fabricated through two steps. First, small panels with a dimension of 40 × 60 × 6.25 mm^3 are printed via FDM technique of the Mark Two. The printed panels are later cut into SBS samples with a dimension of 40 × 12 × 6.25 mm^3 using a band saw. The purpose of the second step is to remove the wall structure of any specimen near the panel edges and eliminate the cutoff effect of the fiber at the start and end of each print path. The burr at the edges of the samples from the cutting process was removed with a belt sander. The dimensions of the SBS specimens are chosen to meet the recommended dimensions in the ASTM D2344

standard [17]. *Figure 5* shows the 3D printed SBS panels and the SBS samples after being cut with the band saw.

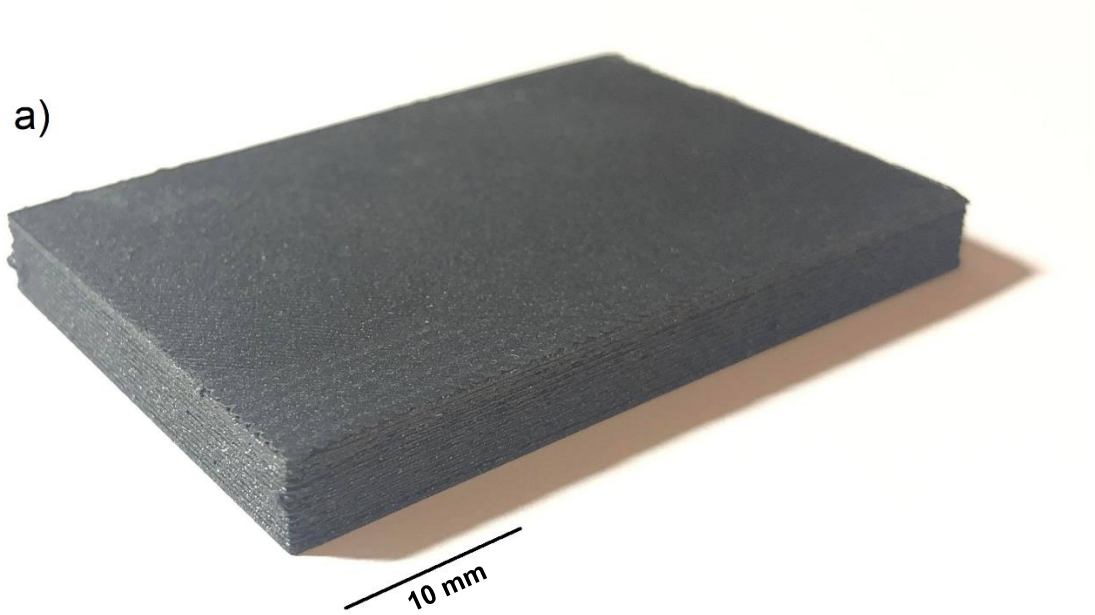

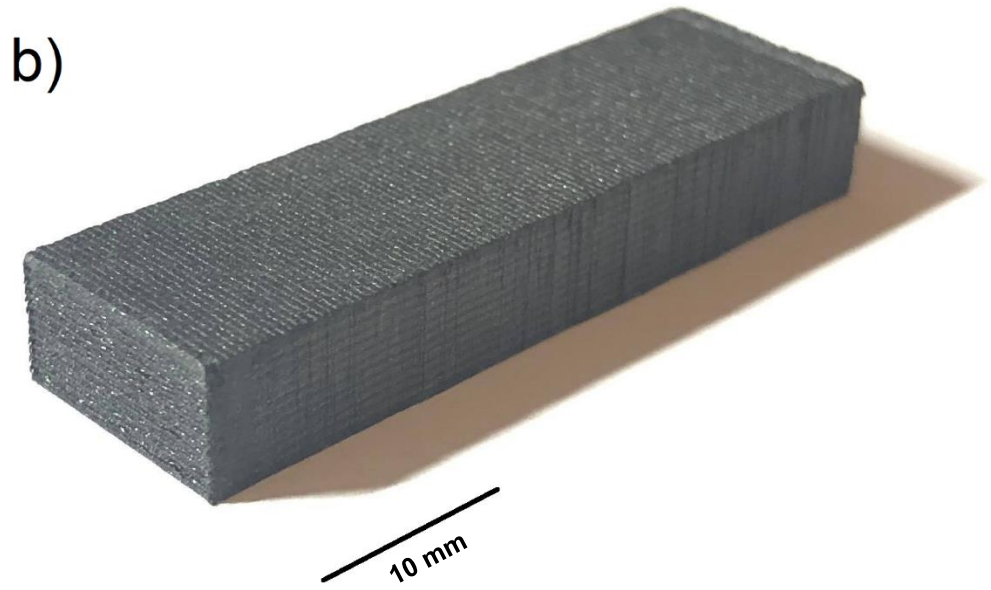

Figure 5: (a) A 3D printed 40 × 60 × 6.25 mm^3 panel, (b) an SBS specimen with dimensions of 40 × 12 × 6.25 mm^3, which was cut with a band saw to eliminate boundary wall effect during ILSS tests

Autoclave process

The samples underwent nine combinations of three temperature levels and three vacuum levels. For each pair of temperature and vacuum, three specimens will be printed and tested. Another three specimens will be printed and tested without the autoclave process. Hence, a total of thirty specimens will be fabricated. The length, width, and thickness of each specimen was measured with a micrometer before and after the autoclave process to evaluate its dimensional accuracy. *Table 1* summarizes the ten batches of samples that were tested and their indexes. For the batch of uncured samples, the autoclave vacuum and temperature were noted as “NA” for not available.

Table 1: Summary of all autoclave processing parameters on SBS specimens

Test Index	C0	C1	C2	C3	C4	C5	C6	C7	C8	C9
Vacuum (kPa)	NA	-10			-50			-90		
Temperature (°C)	NA	130	150	170	130	150	170	130	150	170

The autoclave used in this study is the ASC EC2X4-200P800F. The samples were positioned on an aluminum platform before being transferred into the autoclave for curing. The aluminum platform was treated with two layers of non-stick coating spray. The coating prevented the samples from adhering to the aluminum platform after the cure; hence, the bottom surface of the samples was not damaged upon removal. Sealant tape and a bagging film were used to create a vacuum bag and prevent any air leak. The heat and cooling rates were set to 5°F per minute. The target temperature and vacuum were set according to the desired curing parameters. The curing time was set to 20 minutes for all cures, during which the target temperature and vacuum were maintained. *Figure 6* shows the autoclave curing setup as described.


ASC
a)

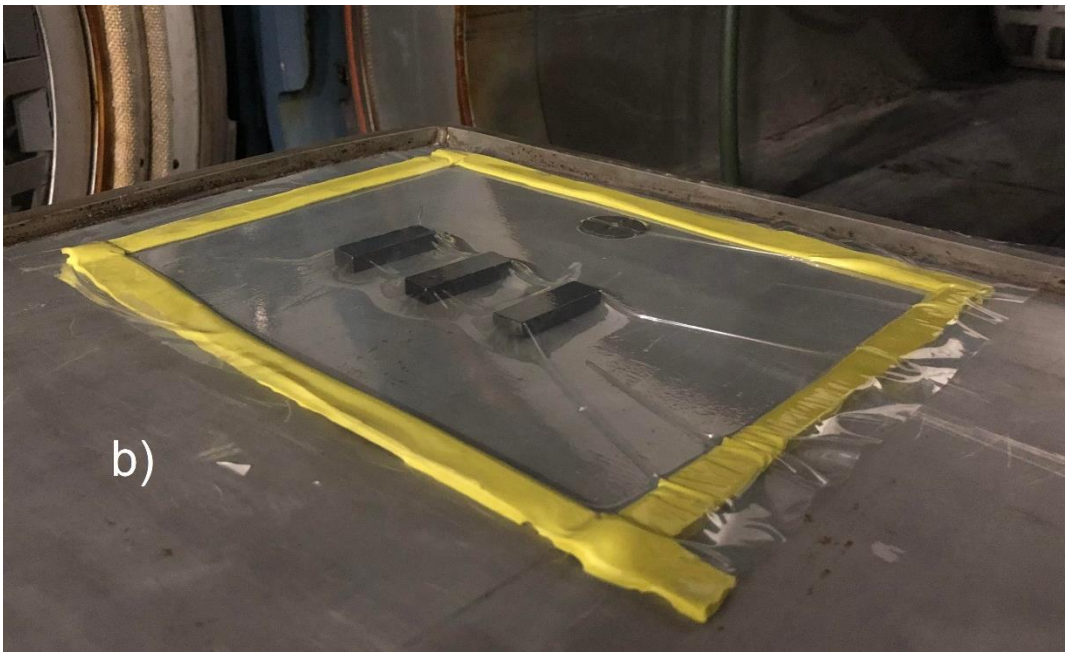
b)

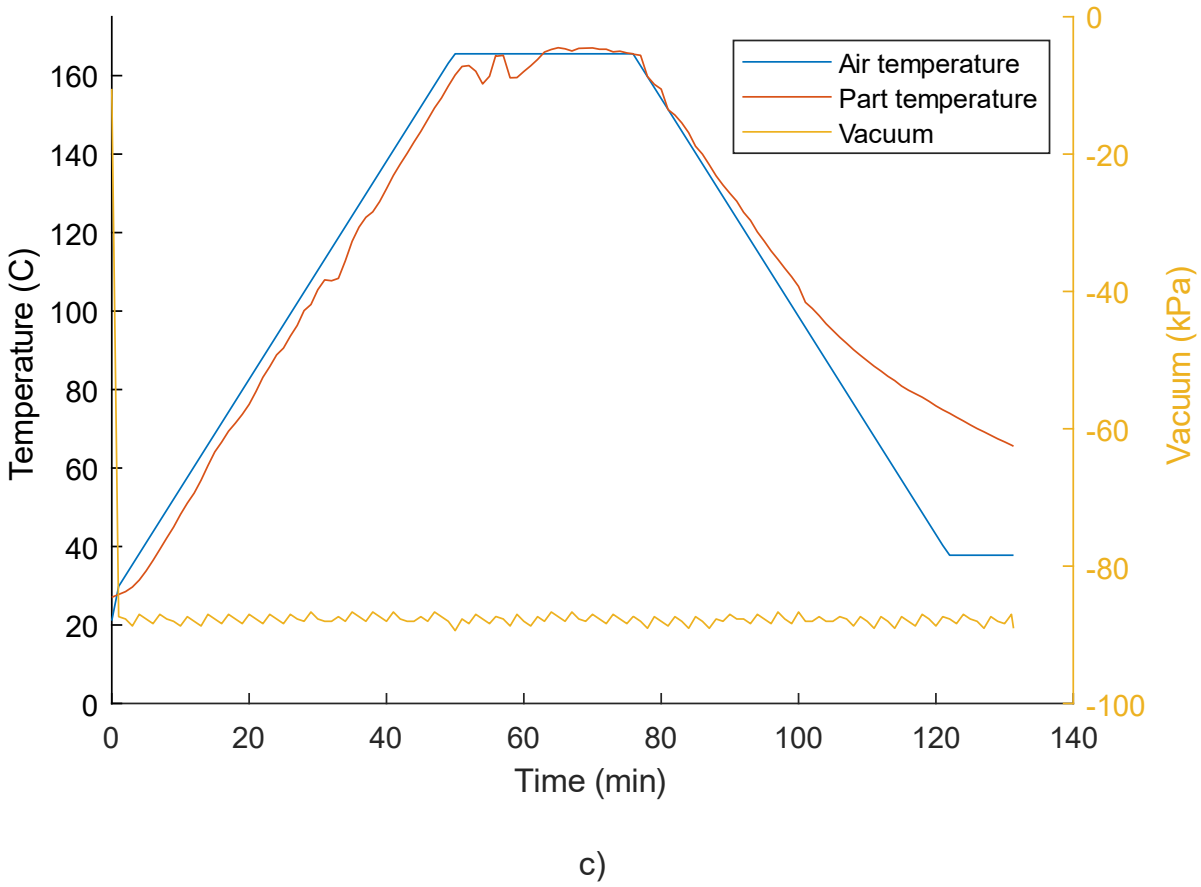

c)

Figure 6: Autoclave curing process setup; a) ASC EC2X4-200P800F autoclave, b) SBS samples positioned on aluminum platform inside a prepared vacuum bag, c) trend view of the autoclave during a cure

Interlaminar shear tests

A universal testing frame (Shimazdu AGS-10kNXD) with a 10 kN load cell and a loading speed of 1 mm/min was used to carry out ILSS tests according to ASTM D2344 standard. The SBS test samples were positioned in a 3-point bend loading setup. *Figure 7* shows the testing setup with a close view of a sample in the 3-point bending configuration. The loading pin was used to apply the displacement at the center of the SBS samples, which were held steady by the side support pins. The support pins are positioned so that the space between them is four times the

thickness of the sample. The interlaminar shear strength of the sample was determined using equation (1) will be used to calculate the ILSS, where P_{max} is the maximum loading force, b and h are the samples' width and thickness:

$$\tau_{ILSS} = \tau_{max} = \frac{3}{4}\frac{P_{max}}{b \cdot h} \quad (1)$$

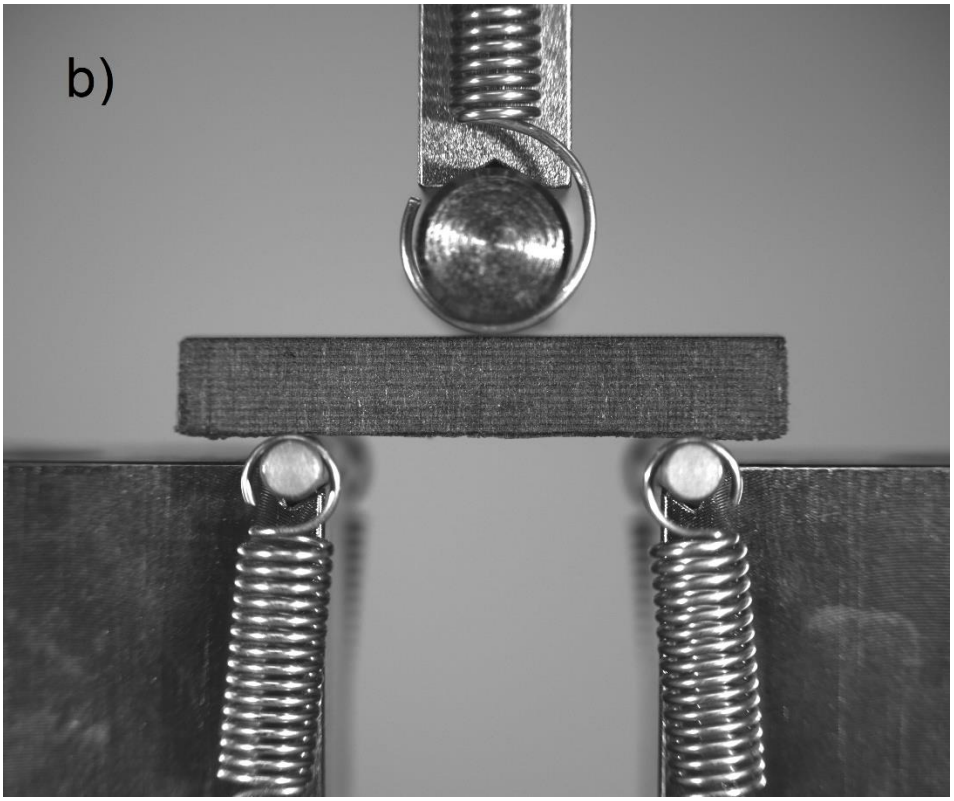

Figure 7: a) ILSS test set up, b) Close view of an SBS samples in 3-point bending configuration

Digital image correlation strain analysis

In Ref. [18], their DIC analysis result showed unsymmetrical stress distribution. This stemmed from the off-centered loading pin and the alignment of the sample on support pins upon damage initiation. This imperfect setup may affect the failure mode of sample due to a higher stress distribution on one side. DIC analysis was attempted in this study to characterize the failure mode of the samples after processing in the autoclave. The samples are loaded into the SBS testing setup as described. The surface of the sample was sprayed with a thin layer of white paint. A high definition camera took pictures at an interval of 1 picture per second while the SBS testing was conducted. The images were cropped in ImageJ and processed in a strain analysis package in MATLAB, Ncorr [19]. *Figure 8* illustrates the user interface of the Ncorr package. To decrease

the processing time, the region of interest was set to only include the portion of the sample between the support pins.

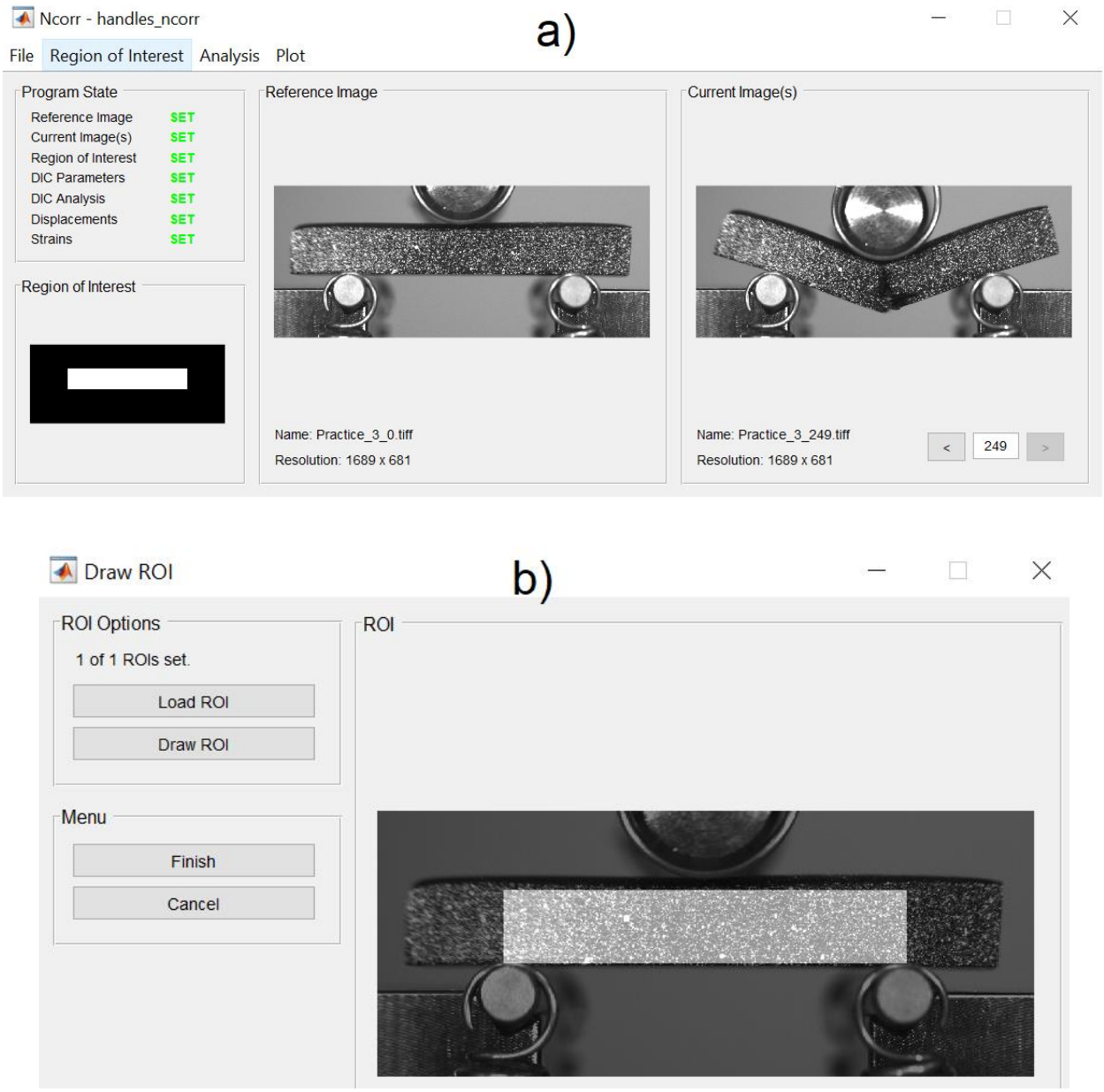

Figure 8: a) Ncorr package user interface, b) region of interest highlighted

4. Results

Effect of different heat rates on ILSS

There are three stages in the curing process: heating, holding, and cooling. The heating stage happened after the samples had been transferred to the autoclave. The samples entered the autoclave at room temperature, approximately 25°C. During the heating stage, the autoclave increased the temperature in the chamber to a target value. According to the manufacturer's datasheet, the maximum heating rate of the autoclave is 2.8°C, or 5°F per minute [20]. Hence, to reach the target temperature of 150°C, the heating stage would take 45 minutes; whereas to reach 170°C, it would take 52 minutes. To investigate the effect of different heating times on the ILSS of the samples, two samples were independently cured at the same target temperature, but with different heating rates. The target temperature was 150°C. The vacuum level was -50 kPa for both cures. The first sample was cured with a heating rate of 2.8°C per minute from room temperature. The heating stage for this cure took 45 minutes. The second cure was set with a heating rate of 1.6°C, or 3°F per minute. The heating stage for this cure took 75 minutes. For both cures, the holding time at 150°C was 20 minutes, and the cooling rate was 2.8°C per minute.

After the cures, the samples were tested to evaluate the ILSS. The force-displacement curves of the two samples are shown in *Figure 9*. From the figure, the maximum forces were retrieved. The force is applied to equation (1) to find the ILSS of the samples cured at 2.8°C and 1.6°C to be 36.87 MPa and 36.6 MPa, respectively. Both curves exhibited similar patterns in their interlaminar shear behavior, including the initial slightly nonlinear portion, the elastic deformation, and the displacement at which the maximum shear stress values were recorded. From these

similarities, it can be concluded that different heating rates have negligible effect on the ILSS of the 3D printed CFRP samples. In other words, the different heating times required for the autoclave to reach different target temperatures did not contribute to the difference in the resulting ILSS values.

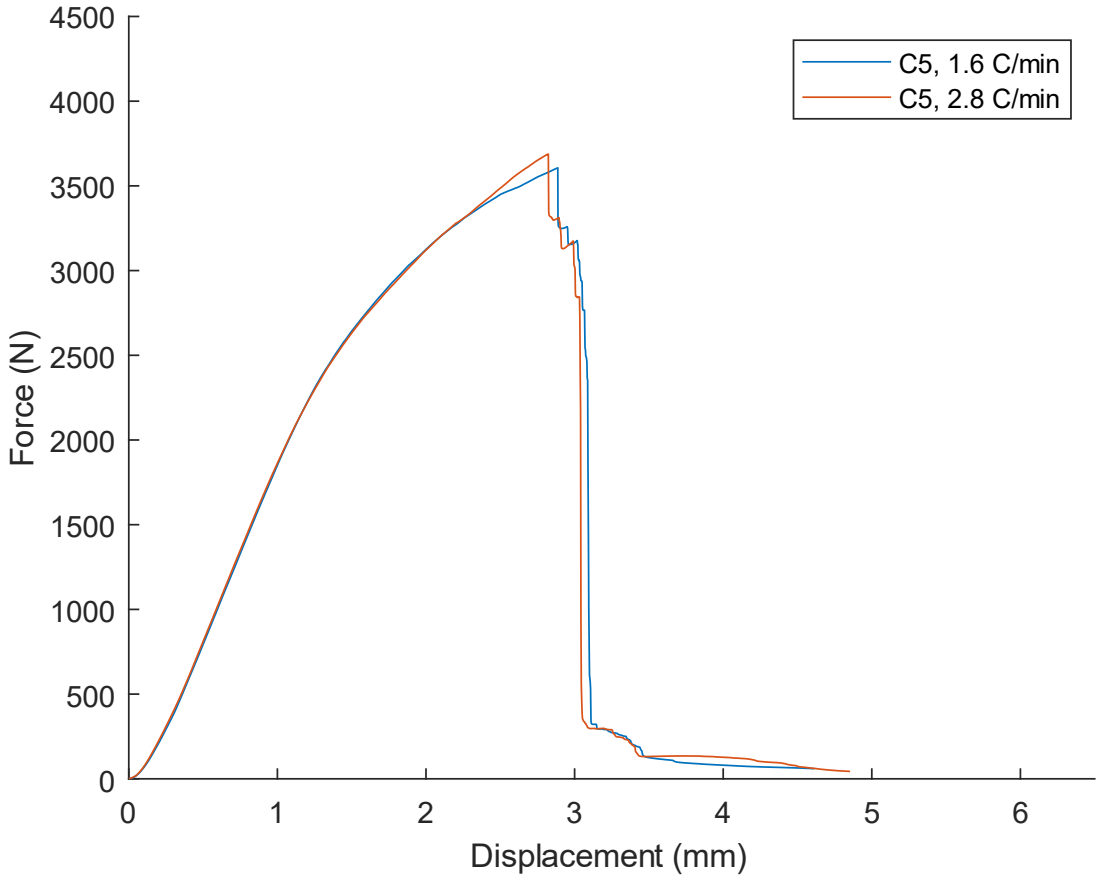

Figure 9: Force-displacement curves of two samples cured with different heating rates

Effect of different temperature and vacuum levels on ILSS

The first batch of samples was printed and tested without undergoing the autoclave process. The purpose of determining the ILSS of uncured samples was to set a reference value to evaluate whether the autoclave process improved the strength of 3D printed CFRP samples. *Figure 10*

illustrates the force-displacement curves of the tested uncured samples. The mean ILSS of uncured samples was 26.58 $\pm$ 1.71 MPa.

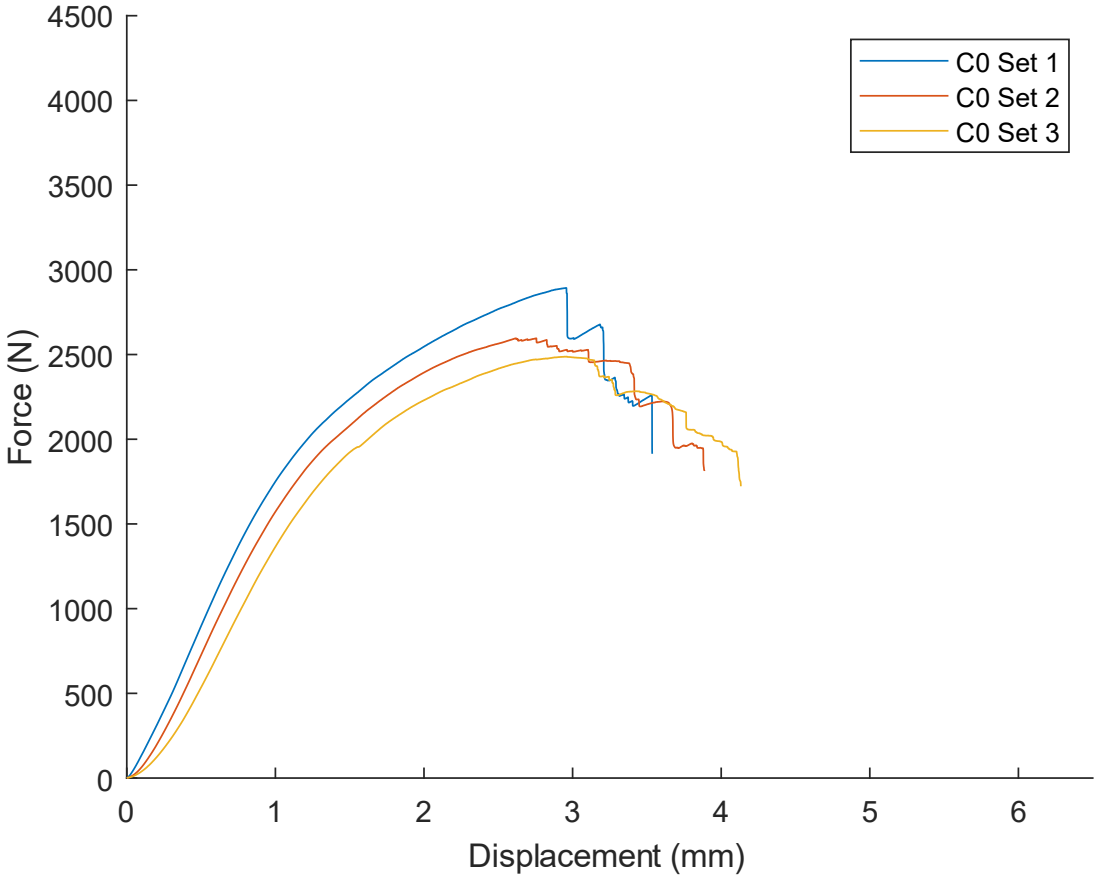

Figure 10: Force-displacement curves of tested uncured CFRP samples

The ILSS of the remaining nine sample batches were also evaluated. Their ILSS values are shown in *Figure 11*. From the figure, samples cured at 130°C exhibited a low ILSS value. At 130°C, and with vacuum levels of -10 kPa and -50 kPa, the ILSS were lower than uncured samples by 3.13% and 4.87%, respectively. This decrease in ILSS performance was attributed to the heat deflection temperature (HDT) of the 3D printed short CFRP. According to Markforged datasheet, the HDT of Onxy is 145°C [21]. With the curing temperature of 130°C, the stiffness of the internal

short CFRP layers did not decrease sufficiently for the interlayer bonds with the continuous CFRP layers to strengthen. The vacuum bag's downward pressure on the sample during curing compressed the thin, continuous CFRP layers together. Due to the unchanged stiffness of the short CFRP layers at 130°C, the crushing force from the short CFRP layers broke the fibers in the continuous CFRP layers. The samples' reduced mechanical performance was caused by the broken fibers. This explains why the ILSS from the C4 cure is lower than the ILSS from the C1 cure. Compared to the C1 cure, the C4 cure's vacuum level exerted a stronger downward pull on the samples' surface. A lower ILSS value was obtained because of more continuous fibers being damaged during C4. However, although C7 experienced a higher level of vacuum, it exhibited an increase in ILSS compared to uncured samples by 1.76%. This increase in ILSS was attributed to the decrease in the voids within the raster pattern of the samples. The -90 kPa vacuum was able to reduce the porosity in the structure of the samples. Further microstructure characterization is needed to quantitively investigate the effectiveness of this vacuum level.

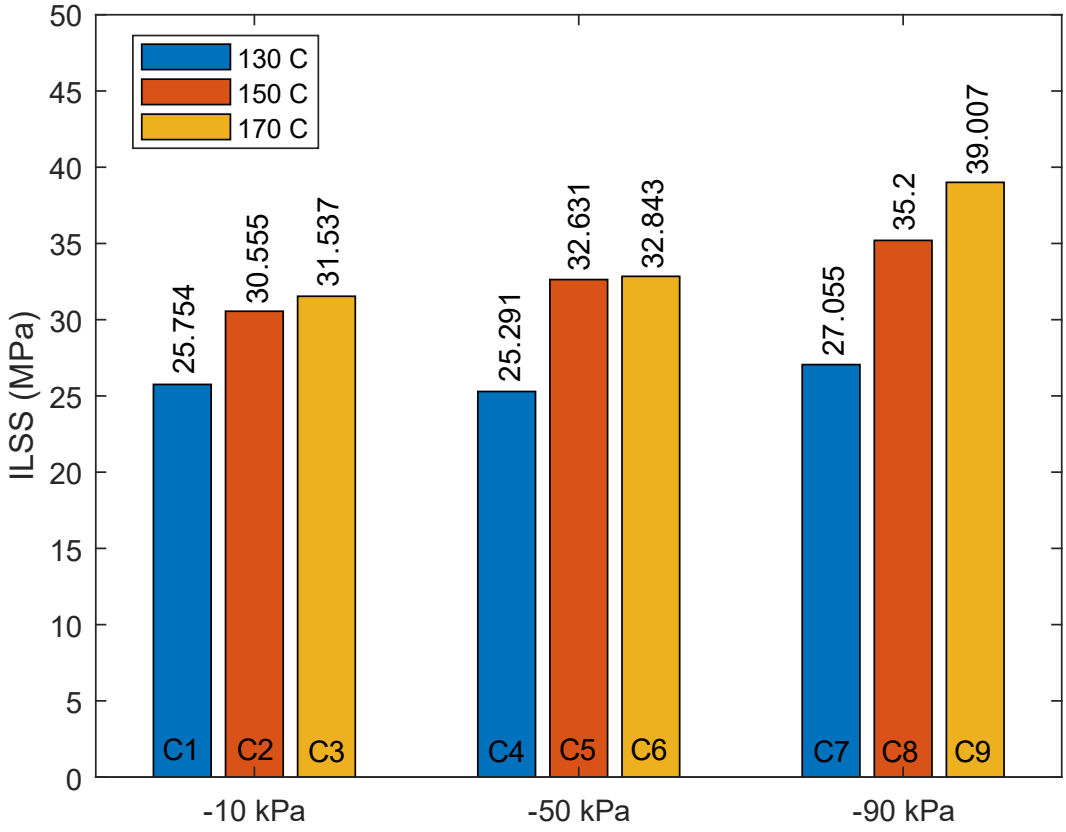

Figure 11: ILSS of CFRP samples after being processed with different autoclave parameters

The ILSS of 3D printed CFRP samples increased considerably when the curing temperature was above 145°C. A proportional relationship is observed between the ILSS and the increase in curing temperature. C9 exhibited the highest ILSS value at 39 MPa, 46.71% improvement compared to uncured samples. *Figure 12* illustrates the force-displacement curves for two samples from the C9 cure. From the figure, a slight nonlinear portion of the curve was observed at the start of the test. This is attributed to the initial contact point of the loading pin and the sample and the between the sample and the support pins. The following linear segment of the curves illustrates the gradual increase of shear stress until the critical stress state. The linear

segment also shows the stiffness of the samples. The stiffness of the samples was estimated by taking the slope of the linear portion of the force-displacement curves. Uncured samples exhibited a stiffness value of 1828 N/mm. The stiffness of samples from C9 cure was evaluated to be 2785 N/mm, a 52.35% increase.

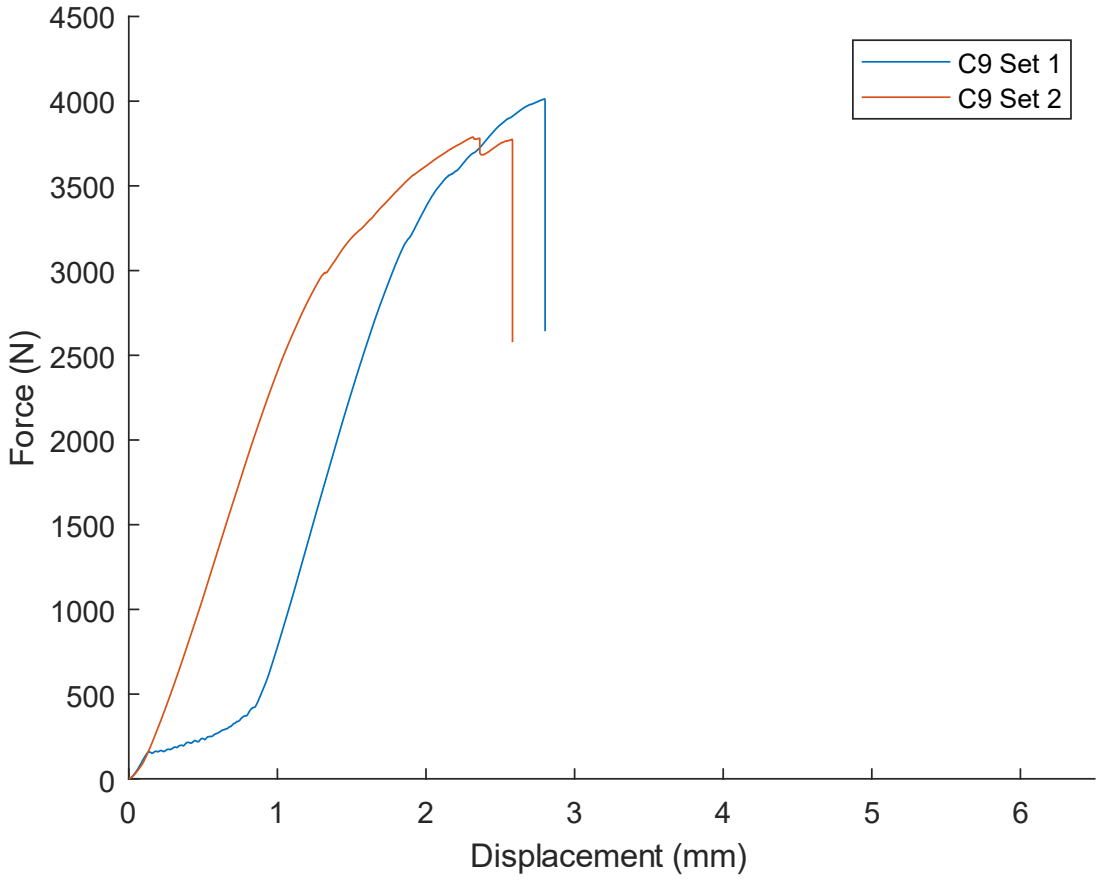

Figure 12: Force-displacement curves of tested CFRP samples cured at 170 C, -90 kPa

From the C0 force-displacement curves in *Figure 10*, the failure of the samples from C0 displays several shear stress drops. This was consistent with the observation from Ref. [18]. In this study, the author performed digital image correlation (DIC) analysis to measure the strain while conducting the ILSS test. At each shear stress drop, the resulting image analysis revealed stress

localization points and their evolution. In comparison to the stress-placement curves from C9-cured samples, the failure happened in only one drop. The second sample for the C9 cure exhibited two drops before the ultimate failure. But after the ultimate failure point, there were no stress drop points. This behavior is an indicator that the interlayer bonds are stronger after the cure. Uncured samples failed in several steps because interlaminar damage occurred and propagated in the matrix material. The one-step failure indicates that the sample performs similarly to a solid body, rather than laminates of composite materials. In other words, the voids in the structure of the sample, between fiber raster and within the CFRP filament, were reduced from the cure.

DIC strain analysis result

The strain field revealed from Ncorr in *Figure 13* shows that the DIC setup has been improved through the symmetry of stress distribution. In Fig. 13d, the force-time curve illustrates the shear stress peaking at time 217.75 seconds. Since the camera was set to capture one image per second, the image at time 217 seconds was retrieved, shown in Fig. 13a. In Fig. 13b, the maximum shear strain points on two sides were identified with the green and red markers. Shear strain was approximately 0 at the vertical center line though the thickness of the sample. Since the loading pin was applied at the center of the sample, the direction of the induced interlaminar shear forces on the left and right side of the loading pin were mirrored through the center line. As shown in Fig. 13b, the directions of the strain run from the support pins to the loading pin, along the length of the sample. The sign of the strain value indicates the oppositeness of the strain responding to the interlaminar forces. The absolute values for shear strain on the left and right side were 0.2361 and 0.2328, respectively. The minor difference between the strain values on the two sides indicates

that the stress was distributed symmetrically. The symmetry in stress distribution helps validate that testing setup for the SBS tests did not cause and the resulting ILSS values.

From the illustrated strain fields, flexural tension and interlaminar shear failure modes can be identified. The analysis could not capture the strain approximate to the damage initiation point. However, as can be seen in Fig. 13a, a crack initiated at the bottom layer of the sample. From the bottom layer, the crack propagated upward through the thickness of the sample. Then, it changed its direction and propagated through between layers. The upward propagation was caused by flexural tension while the change of direction of the crack indicated the occurrence of interlaminar shear failure mode.

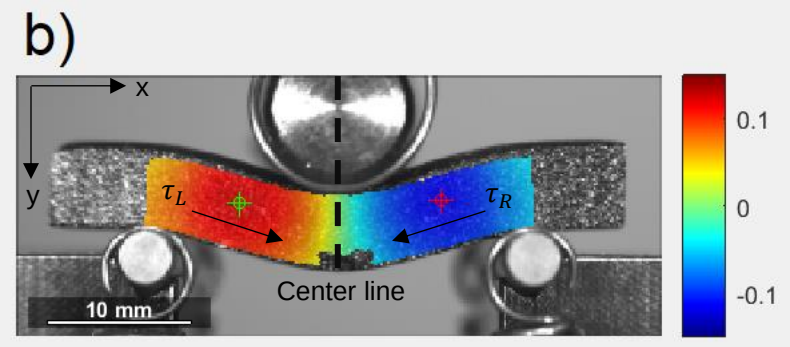
b)
x
y
τ_L
τ_R
Center line
10 mm
0.1
0
-0.1

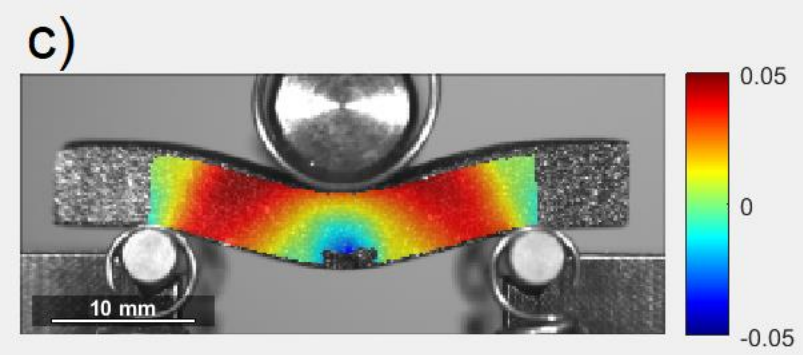
c)
10 mm
0.05
0
-0.05

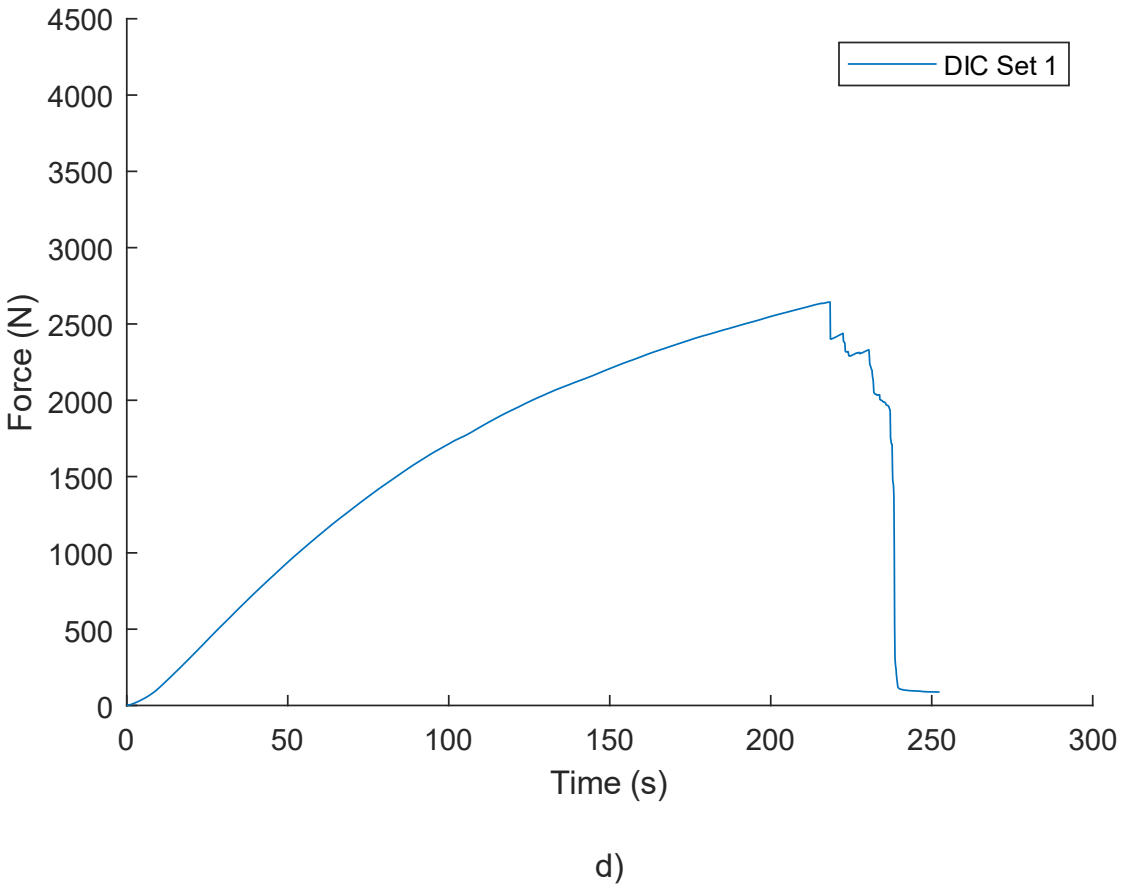

Figure 13: a) DIC sample before failure, b) shear strain ϵ_{xy} evaluation, c) vertical strain ϵ_{yy} evaluation, d) force-time curve of sample used for DIC analysis

5. Conclusions and Future Work

Conclusion Summary

With the results from the ILSS tests, the autoclave process proves to be a viable method to strengthen the interlaminar strength of 3D printed CFRP parts. The method can improve the ILSS by 46% compared to uncured samples. The results revealed that different heating rates had negligible impact in the ILSS. Both curing temperature and vacuum levels have influence over the ILSS value post-curing. A relationship between the increase in temperature and vacuum with the increase in ILSS was observed. Strain analysis revealed a symmetrical stress distribution, proving a better testing setup.

Future Work

The study chose three levels of temperature and three levels of vacuum. The hypothesis was that there would be an optimal curing parameter. The ILSS was hypothesized to increase to a maximum value at such curing parameter, then declined due to the degradation of material from the high temperature of the autoclave process. However, the highest ILSS value was recorded at the most extreme set of temperature and vacuum. Future study can choose finer steps and a larger range in both parameters to capture the optimal curing setting. Statistical methods can also be applied through the ANOVA tests to find how much influence temperature and vacuum has on the ILSS.

Conducting DIC analysis requires a long processing time. Hence, in this study, DIC was only performed on one sample to obtain preliminary strain results. Future work can focus on performing DIC on more samples of different curing settings to find their impacts on shear and

vertical strains. The DIC analysis conducted in this paper can be improved to obtain a more detailed strain field. This includes coating the sample with a finer layer of spray, and tuning the DIC parameters to capture interlaminar displacement as well as the failure location of the sample.

Since DIC analysis can only reveal the behavior of the sample on the outer surfaces, the microstructure of the samples was not characterized. Scanning electron microscopes (SEM) can be employed to examine the interlayer bonds between short and continuous CFRP layers through quantifying the voids between fiber raster. SEM can also be employed to evaluate the pores in the CFRP filaments. This microstructure characterization technique can produce a more direct relationship between post-processing techniques such as autoclave and the resulting mechanical behavior of CFRP parts.

LIST OF REFERENCES

[1] Justo, J., et al. "Characterization of 3D printed long fibre reinforced composites." Composite Structures 185 (2018): 537-548.

[2] Chacón, J. M., et al. "Additive manufacturing of continuous fibre reinforced thermoplastic composites using fused deposition modelling: Effect of process parameters on mechanical properties." Composites science and technology 181 (2019): 107688.

[3] Yu, Tianyu, et al. "Tensile and flexural behaviors of additively manufactured continuous carbon fiber-reinforced polymer composites." Composite Structures 225 (2019): 111147.

[4] He, Qinghao, et al. "3D printed continuous CF/PA6 composites: Effect of microscopic voids on mechanical performance." Composites science and technology 191 (2020): 108077.

[5] Ueda, Masahito, et al. "3D compaction printing of a continuous carbon fiber reinforced thermoplastic." Composites Part A: Applied Science and Manufacturing 137 (2020): 105985.

[6] Ming, Yueke, et al. "Investigation on process parameters of 3D printed continuous carbon fiber-reinforced thermosetting epoxy composites." Additive Manufacturing 33 (2020): 101184.

[7] Bodaghi, M., Cristóvão, C., Gomes, R., Correia, N.C.: Experimental characterization of voids in high fibre volume fraction composites processed by high injection pressure RTM. Compos Part A. Appl. Sci. Manuf. 82,88–99 (2016).

[8] Shi, Kaiwen, et al. "3D printing Kevlar fiber layer distributions and fiber orientations into nylon composites to achieve designable mechanical strength." Additive Manufacturing 39 (2021): 101882.

[9] Van de Werken, Nekoda, et al. "Additively manufactured carbon fiber-reinforced composites: State of the art and perspective." Additive Manufacturing 31 (2020): 100962.

[10] Dickson, Andrew N., et al. "Fabrication of continuous carbon, glass and Kevlar fibre reinforced polymer composites using additive manufacturing." Additive Manufacturing 16 (2017): 146-152.

[11] Dickson, Andrew N., Keri-Ann Ross, and Denis P. Dowling. "Additive manufacturing of woven carbon fibre polymer composites." Composite Structures 206 (2018): 637-643.

[12] Kumar, M. Ajay, M. S. Khan, and S. B. Mishra. "Effect of fused deposition machine parameters on tensile strength of printed carbon fiber reinforced PLA thermoplastics." Materials Today: Proceedings 27 (2020): 1505-1510.

[13] Mei, Hui, et al. "Influence of mixed isotropic fiber angles and hot press on the mechanical properties of 3D printed composites." Additive Manufacturing 27 (2019): 150-158.

[14] Pascual-González, C., et al. "Post-processing effects on microstructure, interlaminar and thermal properties of 3D printed continuous carbon fibre composites." Composites Part B: Engineering 210 (2021): 108652.

[15] Karaş, Büşra, et al. "Additive manufacturing of high density carbon fibre reinforced polymer composites." Additive Manufacturing (2022): 103044.

[16] Guduru, K. K., and G. Srinivasu. "Effect of post treatment on tensile properties of carbon reinforced PLA composite by 3D printing." Materials Today: Proceedings 33 (2020): 5403-5407.

[17] ASTM D2344/D2344M-16. Standard test method for short-beam strength of polymer matrix composite materials and their laminates. West Conshohocken, PA: ASTM International; 2016.

[18] Yavas, Denizhan, et al. "Interlaminar shear behavior of continuous and short carbon fiber reinforced polymer composites fabricated by additive manufacturing." Composites Part B: Engineering 204 (2021): 108460.

[19] Blaber, J., B. Adair, and Antonia Antoniou. "Ncorr: open-source 2D digital image correlation matlab software." Experimental Mechanics 55.6 (2015): 1105-1122.

[20] “Model # ED2X4-200P800F - Technical Specification”. http://www.aschome.com/index.php/en/econoclave-ec2x4. Accessed April 11, 2023.

[21] “Material Datasheet Composites.” Markforged. https://markforged.com/materials/plastics/onyx. Accessed April 11, 2023.